Efficiency enhancement and angle-dependent color change in see-through organic photovoltaics using distributed Bragg reflectors

Wan Jae Dong, Nhat-Truong Lo, Gwan Ho Jung, Juyoung Ham, and Jong-Lam Lee

---

Articles you may be interested in

A comparison of light-coupling into high and low index nanostructured photovoltaic thin films
APL Mater. **3**, 066101 (2015); 10.1063/1.4921955

Nonpolar GaN-based microcavity using Al N ∕ Ga N distributed Bragg reflector
Appl. Phys. Lett. **92**, 061114 (2008); 10.1063/1.2857500

Photovoltaic enhancement of organic solar cells by a bridged donor-acceptor block copolymer approach
Appl. Phys. Lett. **90**, 043117 (2007); 10.1063/1.2437100

All-organic flexible polymer microcavity light-emitting diodes using 3M reflective multilayer polymer mirrors
Appl. Phys. Lett. **87**, 243504 (2005); 10.1063/1.2119416

Si wafer bonded of a - Si ∕ a - Si N x distributed Bragg reflectors for 1.55 - µ m -wavelength vertical cavity surface emitting lasers
J. Appl. Phys. **98**, 043107 (2005); 10.1063/1.2009075

Efficiency enhancement and angle-dependent color change in see-through organic photovoltaics using distributed Bragg reflectors

Wan Jae Dong,[a) Nhat-Truong Lo,[a) Gwan Ho Jung, Juyoung Ham, and Jong-Lam Lee[b)
*Department of Materials Science and Engineering and Division of Advanced Materials Science,
Pohang University of Science and Technology (POSTECH), Pohang, Gyeongbuk 790-784, South Korea*

A distributed Bragg reflector (DBR) is conducted as a bottom reflector in see-through organic photovoltaics (OPVs) with an active layer of poly(3-hexylthiophene) and phenyl-C61-butyric acid methyl ester (P3HT:PCBM). The DBR consists of alternative layers of the high- and low-refractive index materials of Ta_2O_5 (n = 2.16) and SiO_2 (n = 1.46). The DBR selectively reflects the light within a specific wavelength region (490 nm–630 nm) where the absorbance of P3HT:PCBM is maximum. The see-through OPVs fabricated on DBR exhibit efficiency enhancement by 31% compared to the device without DBR. Additionally, the angle-dependent transmittance of DBR is analysed using optical simulation and verified by experimental results. As the incident angle of light increases, peak of reflectance shifts to shorter wavelength and the bandwidth gets narrower. This unique angle-dependent optical properties of DBR allows the facile color change of see-through OPVs. © 2016 AIP Publishing LLC. [http://dx.doi.org/10.1063/1.4943654]

Organic photovoltaics (OPVs) have become one of the most promising candidates for see-through solar cells, since it can be fabricated on transparent substrates and controllable active layer transmittance.[1–4] Various multi-functionalities of see-through OPVs lead to potential applications such as sunroof of automobiles, power-generating windows, and interior decorations.[5–7] The color of see-through OPVs is currently dominated by the materials of active layers. The devices with near-infrared materials with C_{60} fullerene exhibit green color.[3,8] In some specially controlled systems, the grey color has been demonstrated in the devices with complementary absorber materials.[2,3] Not only in the OPVs but also in the dye-sensitized solar cells the transmission spectrum is tuned by employing the absorbing dyes of different colors.[9–11] However, the methods for color tuning by employing different active materials suffer from the difficulties in synthesizing new material with desired absorption spectra and adequate electrical properties.

Microcavity structure on top of an organic active layer was proven to be an effective way for tuning the colors of the see-through OPVs. The microcavity structure consists of the dielectric layer sandwiched between two thin silver films.[12–18] Since the thickness of dielectric layer is a key factor to determine the resonant wavelength in microcavity, monochromatic color across the visible spectrum was demonstrated by controlling the thickness of the dielectric layer.[12] Although the high color purity was achieved by microcavity structures on top of solar cells, the light passed through the microcavity structure cannot be reflected back into the active layer because the bottom electrode is a transparent indium-tin oxide (ITO). This insufficient light absorption in active layer leads to low-efficiency. Moreover, for the practical application of solar cells, the daily rotation of sun

should be considered. Although the color of the see-through OPV is highly sensitive to the angle of incident light, angle-dependent color alternation has not been reported.

In this work, we demonstrate the distributed Bragg reflector (DBR) as a semi-reflective bottom reflector in the see-through OPVs. The DBR which is comprised of alternative layers of Ta_2O_5 and SiO_2 exhibits high reflectance of 98% on the specific wavelength range ($\lambda = 490$–630 nm) where the light absorption of poly(3-hexylthiophene) and phenyl-C61-butyric acid methyl ester (P3HT:PCBM) is maximum. This high reflectance of DBR results in photo-conversion efficiency (PCE) enhancement of OPV by 31% compared to the device without DBR. On the long wavelength region ($\lambda > 630$ nm), optical transmittance of DBR is as high as 80%. A relationship between an incident angle of light and the transmittance of DBR is studied for practical application of solar cells under sunlight (Fig. 1). As the incident angle of light increases, the reflectance band shifts toward short wavelengths. At the high incident angle of light, even the purple light is blocked by DBR, thereby resulting in color change of the transmitted light from purplish to yellowish. This unique optical property allows the multi-color appearance of the see-through OPVs. From these results, the effects of DBR on the efficiency
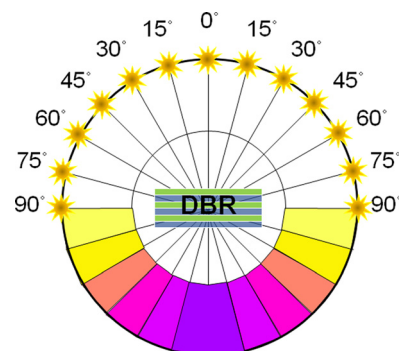

FIG. 1. Color of light transmitted through DBR for various incident angles.

a)W. J. Dong and N.-T. Lo contributed equally to this work.
b)Author to whom correspondence should be addressed. Electronic mail: jllee@postech.ac.kr

enhancement and color-tunability of the see-through OPVs are discussed.

The DBR consists of alternative stacks of quarter-wavelength-thick high and low refractive index layers. As each layer boundary causes a partial reflection of light, the waves with an identical phase form a constructive interference, resulting in a high reflectance. The following equation explains the reflectivity (R) of DBR:[20]

$$R = \left[\frac{n_o(n_2)^{2N} - n_s(n_1)^{2N}}{n_o(n_2)^{2N} + n_o(n_1)^{2N}} \right]^2,$$

where n_o, n_1, n_2, and n_s are the refractive indices of air, two alternating dielectric layers, and the substrate, respectively. N is the number of pairs of DBR. It is notable that a large difference between n_1 and n_2 results in high reflectivity. The refractive indices of the dielectric layers not only determines the reflectivity of DBR but also related to the reflectance bandwidth ($\Delta\lambda_o$) as follows:[20]

$$\Delta\lambda_o = \frac{4\lambda_o}{\pi} \arcsin\left(\frac{n_2 - n_1}{n_2 + n_1} \right),$$

where λ_o is the central wavelength of the band. For the solar cell application, large $\Delta\lambda_o$ is preferred to obtain broadband reflection. Therefore, a large difference in the refractive indices between two dielectric layers is recommended. Consequently, we used a Ta_2O_5 (n = 2.16) and SiO_2 (n = 1.46) as the high- and low-refractive index materials in this work. The thickness and pairs of DBR is optimized experimentally (Figs. S1 and S2).[26] The DBR was deposited on a glass substrate by an alternating layer of Ta_2O_5 (62 nm) and SiO_2 (91 nm), followed by ITO (170 nm) coating using radio-frequency magnetron sputtering. For the control device, the ITO-coated glass substrate (170 nm thick, ~15 Ω/sq) was utilized. As a hole transport layer, Poly(3,4-ethylenedioxythiophene):poly(styrenesulfonate) (PEDOT:PSS) was spin-coated on the ITO layer and dried at 170 °C for 10 min. These substrates were transferred to a N$_2$-filled glove box (<0.1 ppm O2 and H$_2$O). Regioregular poly(3-hexylthiophene) (P3HT, purchased from Rieke Metals and used as received) was first dissolved in 1,2-dichlorobenzene (DCB) to make a 20 mg/ml solution, followed by blending with phenyl-C61-butyric acid methyl ester (PCBM, Nano-C, used as received) in a 3:2 weight ratio. The blend was stirred for ~6 h in a glove box before being spin-coated (700 rpm, 30 s) on top of the prepared substrate. The thickness of an active layer was measured as ~180 nm by a surface profiler. The devices were annealed on a hot plate in a glove box at 130 °C for 10 min. The transparent cathode consisted of Bathocuproine (BCP) (10 nm)/Ag(12 nm)/MoO$_3$(30 nm) was deposited at a base pressure of 1×10^{-6} Torr using the thermal evaporation method.[19] The active device area was ca. 0.06 cm^2. The optical constant of Ta_2O_5 and SiO_2 was measured using spectroscopic ellipsometer (J. A. Woollam Co., Inc., M-44). Commercial software (The Essential Macleod, Thin Film Center, In.), based on what is known as the characteristic matrix method, was employed for optical analysis. The SEM was done using a PHILIPS XL30S with an accelerating voltage of 10 kV and a working distance of 6 mm. The reflection measurement is performed with Agilent

Technologies Cary 4000 UV-Vis spectrometer. The J–V curves were measured under air ambient using a Keithley 2400 source measurement unit. The photocurrent was measured under AM1.5 G 100 mWcm^{-2} illumination from an Oriel 150 W solar simulator. The light intensity was determined using a mono-silicon detector calibrated by the National Renewable Energy Laboratory (NREL). The incident photon to current efficiency (IPCE) is measured using QEX10 Solar Cell Quantum Efficiency Measurement System (PV Measurements, Inc.).

The see-through OPV (Fig. 2(a)) is consisted of glass substrate/DBR/ITO (170 nm)/PEDOT:PSS (30 nm)/P3HT:PCBM (180 nm)/BCP (10 nm)/Ag(12 nm)/MoO$_3$ (30 nm). Light is illuminated on top of the transparent electrode (BCP/Ag/MoO$_3$). The DBR reflects light on the short wavelength region where the absorption of P3HT:PCBM is maximum (Fig. 2(b)). On the other hand, the DBR transmits the light on the long wavelength region (>650 nm), thereby leading to see-through OPVs. Because a large difference in refractive index between the two dielectric materials demonstrates a large reflectance bandwidth of DBR, Ta_2O_5 (n = 2.16) and SiO_2 (n = 1.46) were alternatively deposited on the glass substrate as high- and low- refractive index materials, respectively.[20–23] The Ta_2O_5 layer presents dark-contrast and SiO_2 layer exhibits bright-contrast in the SEM images (Fig. 2(c)) due to a different density of back-scattered electron from each materials. The thickness of Ta_2O_5 layer (62 nm) and SiO_2 layer (91 nm) was predetermined in order to match the central wavelength of the reflectance at 540 nm for an efficient light absorption in the P3HT:PCBM active layer.

In order to design the DBR structure, an optical reflectance was calculated using a commercial software based on the characteristic matrix method. Fig. 3(a) shows the comparison of simulated reflectance and measured reflectance of DBR with 3 pairs, 6 pairs, and 9 pairs of DBR. As the
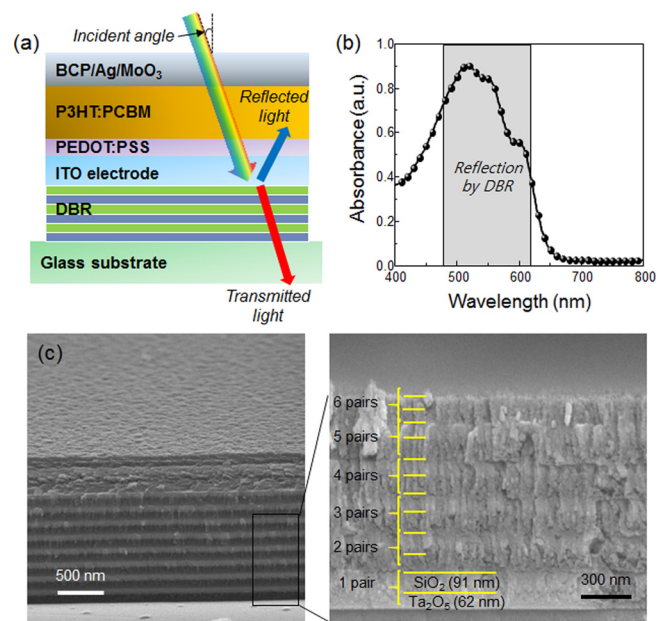

FIG. 2. (a) Schematic device structure of see-through organic photovoltaics with distributed Bragg reflector (DBR). (b) Measured absorbance of P3HT:PCBM active layer. (c) Tilted SEM image (left) and Cross-sectional SEM image (right) of DBR stacks with alternative layers of SiO_2 (91 nm) and Ta_2O_5 (62 nm).
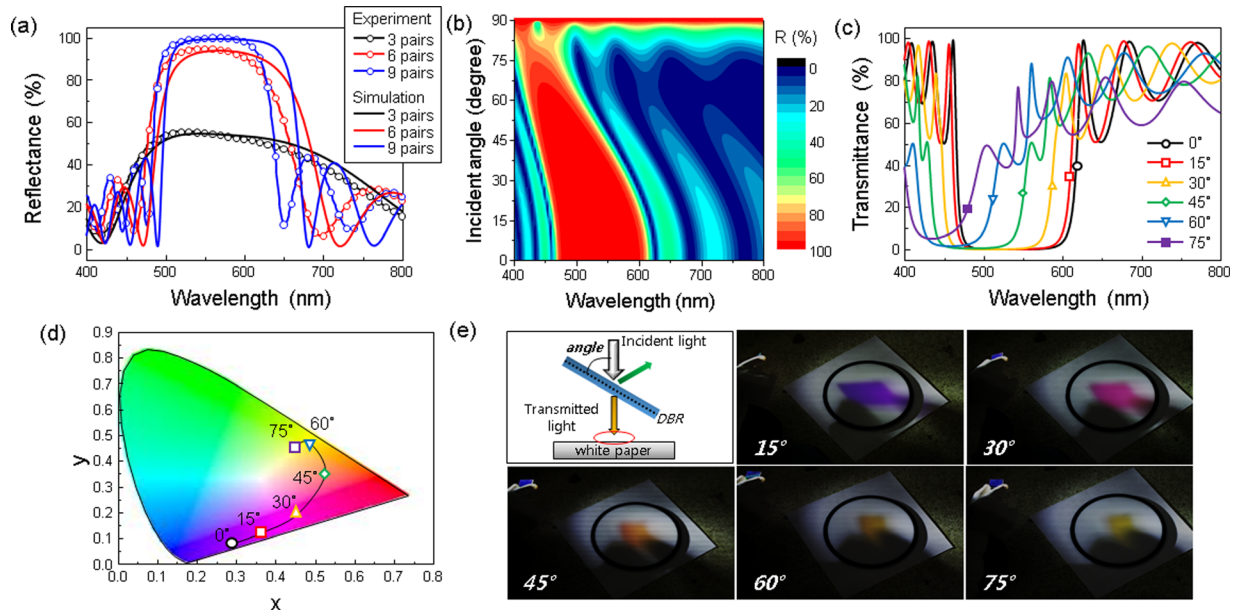
FIG. 3. (a) Experimental and simulated reflectance of DBR having 3, 6, and 9 pairs of SiO2 and Ta2O5. (b) Two-dimensional contour plot of reflectance of DBR (9 pairs) as a function of wavelength and incident angle of light. (c) Transmittance spectra of DBR (9 pairs) for various incident angles. (d) Calculated color coordinates of DBRs with various incident angle of light on the CIE 1931 chromaticity diagram. The incident angles were varied from 0° to 75°. (e) Photograph images of projected light which was transmitted through DBR (9 pairs).

number of stacks increases from 3 to 9 pairs, reflectance greatly increased, approaching 98% at $\lambda = 540$ nm, and the bandwidth gradually decreased from 400 nm to 150 nm. The measured reflectance of DBR is in good agreement with the calculated one. But a slight variation exists because of the low refractive index of Ta_2O_5 (n = 2.16) which is smaller than the ideal value (n = 2.3). The deposition conditions were manipulated to increase the refractive index of Ta_2O_5 and the resultant value was 2.16 (Fig. S3).[26] We believe this low refractive index is resulted from the low density of the film due to insufficient adatom mobility during the low temperature deposition.[24,25] Since an optical thickness of DBR is highly dependent on the incident angle of light, the reflectance and transmittance spectrum can be easily changed. In order to find the relationship between optical properties of DBR and incident angle of light, reflectance contour of 9-pair DBR was simulated as a function of incident angle and wavelength (Fig. 3(b)). As the incident angle increases, reflectance band shifts toward short wavelength region and bandwidth gets narrower. Note that the DBR shows the high reflectance about 90% even at high incident angle of 75°. This result confirms the effectiveness of DBR as a broad angle reflector. We compare the relationship between incident angle of light and transmittance of the DBR (Fig. 3(c)). At the incident angle of 0°, the stop-band wavelength ranges from 470 nm to 620 nm with a central wavelength at 540 nm. As the incident angle increases from 0° to 75°, the central wavelength gradually moves to 420 nm and the stop-bandwidth shrinks from 150 nm to 80 nm. This large change in the transmittance spectrum results in a dramatic color alternation (Fig. 3(d)). With the increase in the incident angle of light, color changes from purplish to yellowish (anticlockwise in the CIE diagram). In order to verify the accuracy of calculated result, the photographs of the transmitted light through DBR were captured as a function of incident angle of light
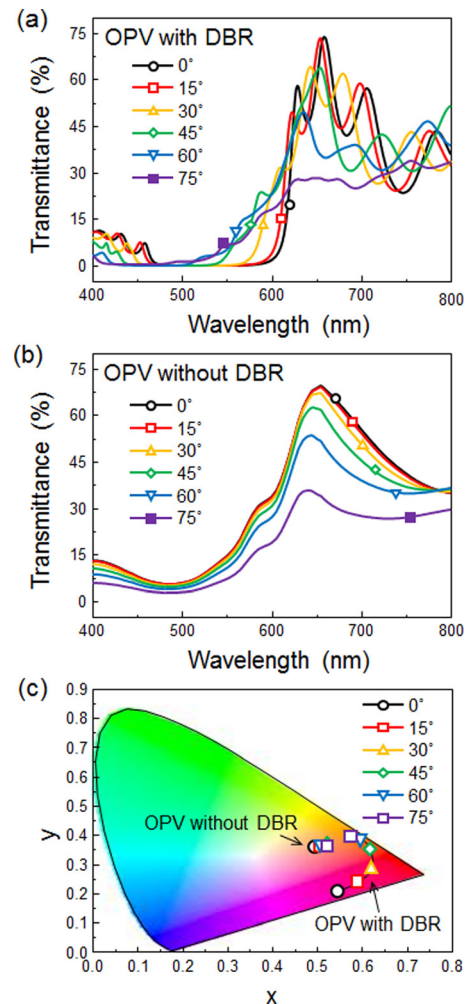

FIG. 4. Calculated transmittance spectra of OPVs (a) with DBR and (b) without DBR for the incident angle from 0° to 75°. (c) CIE 1931 coordinates of transmitted light through OPVs with DBR and without DBR for the various incident angles of light.
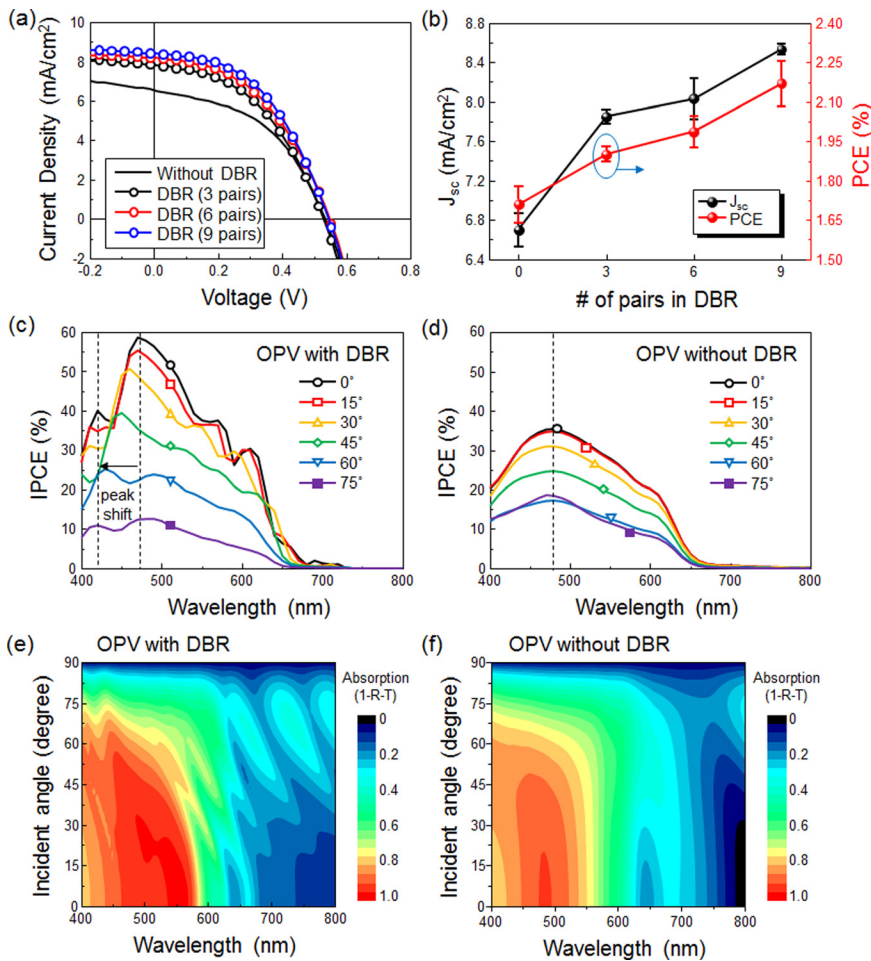
FIG. 5. (a) J-V characteristics of devices without DBR, 3 pairs, 6 pairs, and 9 pairs of DBR. (b) J_{sc} and PCE is plotted as a function of the number of pairs in DBR. IPCE spectra of OPVs (c) with DBR and (d) without DBR. Simulated two-dimensional contour plot of light absorption as a function of incident angle and wavelength in OPVs (e) with DBR and (f) without DBR.

(Fig. 3(e)). The transmitted light with small incident angles of 15° shows purplish color due to a relatively high optical transmittance on a short wavelength region (<450 nm). In the case of incident angle of 30°, the transmitted light exhibits the magenta color which is mixed by a blue (400 < λ < 450 nm) and red light (>600 nm). When the light is illuminated on DBR with the high incident angle of 60° and 75°, orange and yellowish colors were presented, respectively. These results show a good agreement with the calculated color coordination.

The simulated transmittance spectra of the see-through OPVs with DBR (Fig. 4(a)) and without DBR (Fig. 4(b)) are presented for various incident angles of light. At the incident angle of 0°, the OPVs with DBR exhibit much lower transmittance on the short wavelength region (400–600 nm) than the OPVs without DBR, because the DBR effectively reflects the light into the P3HT:PCBM active layer. But, on the long wavelength region (>600 nm,), the DBR allows the light to pass through the OPVs, thereby resulting in high optical transmittance of 43% which is comparable to the device without DBR (51%). In addition, the stop-band of OPVs with DBR shifts as large as 95 nm when the incident angle of light is changed from 0° to 75°, while no shift of transmittance spectra was observed for the device without DBR. The calculated color of the see-through OPVs is plotted in the CIE chromaticity diagram (Fig. 4(c)). With the increase in the incident angle of light, the OPVs with DBR show the color alternation from magenta to yellowish (anticlockwise in the CIE diagram). But the OPVs without DBR did not

show any change in the CIE coordination, meaning that there is no color tunability.

To verify the effect of DBR on the performance of the see-through OPVs, devices were fabricated on the glass substrate and the J-V characteristics are shown in Fig. 5(a). The cell on the ITO-coated glass substrate exhibits open-circuit voltage (V_{oc}) = 0.52 V, short-circuit current (J_{sc}) = 6.6 mA/cm², fill factor (FF) = 46.6%, and PCE = 1.64%. The low efficiency was attributed to low J_{sc}, which comes from the insufficient light absorption in the P3HT:PCBM active layer. On the other hand, when the DBRs with 3 pairs, 6 pairs, and 9 pairs are employed as a back reflector, the J_{sc} increases to 7.8 mA/cm², 8.1 mA/cm², and 8.4 mA/cm², respectively (summarized in Table I). As a result, the OPV with 9 pairs of DBR shows the highest efficiency of 2.15%. The V_{oc} and FF do not change with the DBR structure, meaning that the DBR structure does not participate in electrical properties of

TABLE I. Photovoltaic performances of the devices on ITO-coated glass and DBR-coated glass substrates. The light condition was AM 1.5 G 100 mW/cm² illuminations for the measurements.

Substrate	V_{OC} (V)	J_{SC} (mA/cm²)	FF (%)	PCE (%) (averaged PCE)
Glass	0.53	6.6	46.6	1.64 (1.71)
Glass/DBR (3 pairs)	0.53	7.8	45.2	1.88 (1.90)
Glass/DBR (6 pairs)	0.55	8.1	44.7	2.00 (1.99)
Glass/DBR (9 pairs)	0.55	8.4	46.3	2.15 (2.17)

the OPVs. The small J_{sc} and FF of the see-through OPVs with the BCP/Ag/MoO$_3$ cathode could be originated from the small average transmittance (400–700 nm) of the BCP/Ag/MoO$_3$ cathode (76.9%, measured) as well as the low electrical conductivity ($\sim 1.1 \times 10^7$ S/m, measured). The transmittance is smaller than ITO/PEDOT:PSS (87.5%, measured) and electrical conductivity is also smaller than the conventional reflective cathode of LiF/Al (1/100 nm) (3.2×10^7 S/m, measured). We believe that both J_{sc} and FF could be improved through optimization of transmittance and conductivity of BCP/Ag/MoO$_3$. The statistical results of Jsc and PCE are plotted as a function of number of pairs in DBR (Fig. 5(b)). The averaged PCE increases with the number of pairs of DBR, from 1.71% for bare-ITO film to 1.90% (3 pairs of DBR), 1.99% (6 pairs), and 2.17% (9 pairs). This increase of PCE originates from the increase of J_{sc}. This provides the evidence that DBR significantly affects the increase of J_{sc}, leading to the enhancement of PCE in the OPVs. The IPCE in Figs. 5(c) and 5(d) was measured to identify the wavelength- and incident angle-dependency of device performances. At the incident angle of 0°, the IPCE of OPVs with DBR (Fig. 5(c)) presents a superior performance on the visible spectrum compared to the device without DBR (Fig. 5(d)), because the DBR effectively reflects the light into the P3HT:PCBM active layer. As the incident angle of light increases from 0° to 75°, the peaks gradually shift from 470 nm to 420 nm for the device with DBR. On the other hand, the solar cells without DBR indicate no shift in the IPCE spectra with the incident angle of light. A two-dimensional contour of light absorption in the OPVs was simulated as a function of incident angle and wavelength for the OPVs with DBR (Fig. 5(e)) and without DBR (Fig. 5(f)). The device with DBR shows higher intensity of light absorption on the short wavelength region (400 nm $< \lambda <$ 590 nm) than the OPV without DBR. As the incident angle of light increases, the DBR makes the absorption band of OPV narrower and shifts toward the short wavelength region. But there was no peak-shift in light absorption in OPV without DBR (Fig. 5(f)). This simulated absorption spectrum coincides with the experimental results.

In summary, we have demonstrated efficient enhancement of the see-through OPVs by employing the DBR as the bottom reflector. The DBR selectively reflects the light within bandwidth ranges from 470 nm to 620 nm, while the photons with a long wavelength >600 nm transmits through DBR. Therefore, both strong light harvesting and optical transparency were simultaneously achieved in the see-through OPVs. The PCE of the see-through OPVs with the optimized DBR is enhanced by 31% compared to the device without DBR. Furthermore, the relationship between the incident angle of light and color change was comprehensively studied. The reflectance band of DBR shifted to shorter wavelengths with the incident angle of light, thereby leading to angle-dependent color alternation of see-through OPVs. When the materials with low absorption coefficient are employed as an active layer, the angle-dependent color tunability of the see-through OPVs would further be improved.

[1]L. Dou, W.-H. Chang, J. Gao, C.-C. Chen, J. You, and Y. Yang, Adv. Mater. **25**, 825 (2013).

[2]K.-S. Chen, J.-F. Salinas, H.-L. Yip, L. Huo, J. Hou, and A. K.-Y. Jen, Energy Environ. Sci. **5**, 9551 (2012).

[3]H.-W. Lin, Y.-H. Chen, Z.-Y. Huang, C.-W. Chen, L.-Y. Lin, F. Lin, and K.-T. Wong, Org. Electron. **13**, 1722 (2012).

[4]C.-C. Chen, L. Dou, R. Zhu, C.-H. Chung, T.-B. Song, Y. B. Zheng, S. Hawks, G. Li, P. S. Weiss, and Y. Yang, ACS Nano **6**, 7185 (2012).

[5]A. Colsmann, A. Puetz, A. Bauer, J. Hanisch, E. Ahlswede, and U. Lemmer, Adv. Energy Mater. **1**, 599 (2011).

[6]B. Norton, P. C. Eames, T. K. Mallick, M. J. Huang, S. J. McCormack, J. D. Mondol, and Y. G. Yohanis, Sol. Energy **85**, 1629 (2011).

[7]R. R. Lunt and V. Bulovic, Appl. Phys. Lett. **98**, 113305 (2011).

[8]J. Meiss, F. Holzmueller, R. Gresser, K. Leo, and M. Riede, Appl. Phys. Lett. **99**, 193307 (2011).

[9]D. Kumaresan, R. P. Thummel, T. Bura, G. Ulrich, and R. Ziessel, Chem. Eur. J. **15**, 6335 (2009).

[10]K. Zhang, C. Qin, X. Yang, A. Islam, S. Zhang, H. Chen, and L. Han, Adv. Energy Mater. **4**, 1301966 (2014).

[11]Y. Zhao, G. A. Meek, B. G. Levine, and R. R. Lunt, Adv. Opt. Mater. **2**, 606 (2014).

[12]Y.-H. Chen, C.-W. Chen, Z.-Y. Huang, W.-C. Lin, L.-Y. Lin, F. Lin, K.-T. Wong, and H.-W. Lin, Adv. Mater. **26**, 1129 (2014).

[13]K.-T. Lee, S. Seo, J. Y. Lee, and L. J. Guo, Adv. Mater. **26**, 6324 (2014).

[14]Y.-K. R. Wu, A. E. Hollowell, C. Zhang, and L. J. Guo, Sci. Rep. **3**, 1194 (2013).

[15]M. A. Kats, R. Blanchard, P. Genevet, and F. Capasso, Nat. Mater. **12**, 20 (2013).

[16]B. Valle, S. Loser, J. W. Hennek, V. DeGeorge, C. Klosterman, J. H. Andrews, K. D. Singer, and T. J. Marks, Opt. Express **20**, A954 (2012).

[17]S. Loser, B. Valle, K. A. Luck, C. K. Song, G. Ogien, M. C. Hersam, K. D. Singer, and T. J. Marks, Adv. Energy Mater. **4**, 1301938 (2014).

[18]K.-S. Chen, H.-L. Yip, J.-F. Salinas, Y.-X. Xu, C.-C. Chueh, and A. K.-Y. Jen, Adv. Mater. **26**, 3349 (2014).

[19]G. H. Jung, K. Hong, W. J. Dong, S. Kim, and J.-L. Lee, Adv. Energy. Mater. **1**, 1023 (2011).

[20]S. O. Kasap, *Optoelectronics and Photonics: Principles and Practices*, 2nd ed. (Prentice Hall, New Jersey, 2001).

[21]D. P. Puzzo, M. G. Helander, P. G. O'Brien, Z. Wang, N. Soheilnia, N. Kherani, Z. Lu, and G. A. Ozin, Nano Lett. **11**, 1457 (2011).

[22]J. W. Leem and J. S. Yu, Opt. Express **20**, 20576 (2012).

[23]M. F. Schubert, J.-Q. Xi, J. K. Kim, and E. F. Schubert, Appl. Phys. Lett. **90**, 141115 (2007).

[24]A. K. Chu, H. C. Lin, and W. H. Cheng, J. Electron. Mater. **26**, 889 (1997).

[25]K. Hong, H. K. Yu, I. Lee, K. Kim, S. Kim, and J.-L. Lee, Adv. Mater. **22**, 4890 (2010).

[26]See supplementary material at http://dx.doi.org/10.1063/1.4943654 for simulated reflectance of DBR and measured refractive indices of Ta$_2$O$_5$.